Michelle Delco   ORCID iD: 0000-0003-0973-2075

Mitoprotective therapy prevents rapid, strain-dependent mitochondrial dysfunction after articular cartilage injury

Lena R. Bartell[1], Lisa A. Fortier[2], Lawrence J. Bonassar[3, 4], Hazel H. Szeto[5], Itai Cohen[6], and Michelle L. Delco[2]*

[1] School of Applied & Engineering Physics, Cornell University, Ithaca, NY, United States of America

[2] Department of Clinical Sciences, Cornell University, Ithaca, NY, United States of America

[3] Sibley School of Mechanical and Aerospace Engineering, Cornell University, Ithaca, NY, United States of America

[4] Meinig School of Biomedical Engineering, Cornell University, Ithaca, NY, United States of America

[5] Burke Medical Research Institute, White Plains, NY, United States of America

[6] Department of Physics, Cornell University, Ithaca, NY, United States of America

*Corresponding author
Michelle L. Delco, DVM, PhD
Veterinary Medical Center C2-001
930 Campus Road
Cornell University
Ithaca, NY 14853
Phone: (607) 253-3100
Fax: (607) 253-3102
e-mail: mld12@cornell.edu

Author Contributions:

MLD and LRB are responsible for conception and design of the study, developed the methodologies, performed the experiments and drafted the article. All authors contributed intellectual content, participated in analysis and interpretation of the data, provided critical revision and approve the final submitted version of the manuscript.

Running Title: Strain-dependent mitochondrial dysfunction in cartilage

ABSTRACT

Post-traumatic osteoarthritis (PTOA) involves the mechanical and biological deterioration of articular cartilage that occurs following joint injury. PTOA is a growing problem in healthcare due to the lack of effective therapies combined with an aging population with high activity levels. Recently, acute mitochondrial dysfunction and altered cellular respiration have been associated with cartilage degeneration after injury. This finding is particularly important because recently-developed mitoprotective drugs, including SS-peptides, can preserve mitochondrial structure and function after acute injury in other tissues. It is not known, however, if cartilage injury induces rapid structural changes in mitochondria, to what degree mitochondrial dysfunction in cartilage depends on the mechanics of injury, or the time frame over which such dysfunction develops. Similarly, it is unknown if SS peptide treatment can preserve mitochondrial structure and function after cartilage injury. Here, we combined fast-camera elastography, longitudinal fluorescence assays, and computer vision techniques to track the fates of thousands of individual cells. Our results show that impact induces mechanically-dependent mitochondrial depolarization within a few minutes after injury. Electron microscopy revealed that impact induces rapid structural changes in mitochondria that are related to reduced mitochondrial function, namely fission and loss of cristae structure. We found that SS-peptide treatment prior to impact protects mitochondrial structure and preserves mitochondrial function at levels comparable to that of unimpacted control samples. Overall, this study reveals the vital role of mitochondria in mediating cartilage's peracute (within minutes) response to traumatic injury and

demonstrates mitoprotection as a promising therapeutic strategy for injury-induced cartilage damage.

Key Words: Mitoprotection, mitochondria, mechanotransduction, cartilage impact, posttraumatic osteoarthritis

INTRODUCTION

Osteoarthritis (OA) is a common cause of disability with a growing prevalence as the population ages, yet no therapeutics are available to prevent this disease.[1,2] A hallmark of OA is the mechanical and biological deterioration of articular cartilage, which provides load dissipation and a low friction surface for joint motion.[3] Articular cartilage is composed primarily of a dense, poro-viscoelastic extracellular matrix and chondrocytes, the sole cell type. Chondrocyte function is regulated in part by mechanical stimuli, where moderate loading initiates beneficial anabolic responses including synthesis of matrix proteins, but rapid or excessive loading induces cell death and catabolic signaling that lead to cartilage matrix degradation.[4-7] Although loading is known to play this critical role in cartilage homeostasis, the mechanisms by which mechanical injury leads to cartilage damage and PTOA initiation have not been fully elucidated. In particular, although cellular responses in the acute time frame (hours to days) after injury have been investigated,[8] immediate and peracute (minutes to hours) events are less well understood.

Importantly, mounting evidence suggests that mitochondria are central mediators of the early cellular response to cartilage injury. Mitochondrial respiratory dysfunction is known to occur in late stage OA and early-chronic OA,[9-11] and has been observed within several hours after injury.[12] Oxidative stress and apoptosis have also been observed as

acute responses to cartilage injury and can be mediated by mitochondria, as observed in a variety of experimental models,[8, 11-22] and such mitochondrial responses have been targeted to mitigate PTOA in a porcine model.[23] However, the kinetics of mitochondrial dysfunction in the peracute time frame after injury remain unknown. Additionally, mitochondria are mechanically connected to their intra- and extra-cellular environment, and are sensitive to their mechanical environment, but their role during acute cartilage injury has not been established.[17] In vivo, lubricin-deficient mice with increased whole-joint friction displayed evidence of mitochondrial dysregulation, including increased reactive oxygen species and caspase activation.[22] Furthermore, an *ex vivo* wear model recently revealed that mitochondrial dysfunction is related to increased friction and sliding strain at the articular surface,[20] but it remains unknown if a similar response develops immediately after rapid injurious loading or to what degree such mitochondrial dysfunction depends on injury mechanics.

Injury-induced mitochondrial dysfunction in cartilage is especially interesting because it may present a promising therapeutic target. Broadly, mitochondrial function relies on the electron transport chain (ETC) to build an electrochemical gradient, or polarization, across the inner membrane, which in turn drives energy production. As such, loss of the characteristic folded cristae structure and depolarization of the inner mitochondrial membrane are hallmarks of mitochondrial dysfunction and are observed in mitochondria-mediated diseases.[24] Recently-developed mitoprotective SS-peptides localize to the inner mitochondria membrane, where they stabilize and restore mitochondrial structure and function.[25] SS-31 (Bandavia, Elamipretide; Stealth BioTherapeutics, Newton MA) targets cardiolipin, a phospholipid exclusively expressed on the inner mitochondrial membrane

that promotes christae structure and efficient electron transport. By preventing oxidation of cardiolipin, SS-31 improves mitochondrial coupling (reducing reactive oxygen species and increasing ATP production) and prevents cell death and apoptosis.[25-29] Indeed, SS-peptides have shown promise for treating other mechanically-induced, mitochondria-mediated diseases and are currently in clinical trials for multiple disease including ischemia reperfusion injury and pressure-induced retinopathy.[28, 30-32] Previous work by our group demonstrated that SS-31 can prevent chondrocyte death and cartilage matrix degradation,[15] but it the effect of SS-peptides on chondrocyte mitochondrial structure and function immediately after mechanical injury is unknown.

Understanding how chondrocyte mitochondria respond to their mechanical environment during injury requires observing both the mechanical and biological response of cartilage at high spatial and temporal resolution, which presents a challenge experimentally. Impact loading must be rapid to be considered injurious[33] and cartilage material properties vary over tens of microns.[34, 35] Thus, to observe local tissue deformation *in situ* during injurious loading, data must be collected at rates of ~1,000 points per second and with micron-scale spatial resolution. A fast-camera elastography technique was recently developed to enable this rapid mechanical analysis.[36] Additionally, to observe peracute chondrocyte function, individual cells' behavior must be tracked over time with a temporal resolution of minutes, which could be accomplished using optical microscopy and fluorescent probes. Testing the mechanical dependence of peracute mitochondrial dysfunction after cartilage impact would require combining all of these techniques to observe chondrocytes *in situ* during injurious loading.

In this study, we considered two hypotheses: first that cartilage impact induces rapid, mechanically-dependent mitochondrial dysfunction and second, that SS-peptides protect mitochondrial structure and function after injury. To test these hypotheses, we combined advanced techniques from both mechanics and biology to reveal the complex relationship between injurious loading and individual chondrocyte behavior. In particular, we used longitudinal confocal microscopy with computer vision analysis to track a large number of individual chondrocytes in an *ex vivo* injury model and correlated their behavior with local injury mechanics obtained via fast camera elastography. We further utilized electron microscopy to confirm structural and morphological changes in mitochondria and observed how all of the responses changed with mitoprotective treatment.

METHODS

Sample Preparation

Neonatal bovine stifles were obtained from a local abattoir (Gold Medal Packing, Rome, NY) within 24 hours of sacrifice. Cylindrical explants (6 mm diameter, 3 mm deep including articular surface) were dissected sterilely from the apex of the medial femoral condyle (1 explant/animal, N=9 animals; Figure 1a). Cylinders were cultured (37°C, 21% O_2, 5% CO_2) for ~8 hours in media (phenol-free DMEM containing 1% FBS, HEPES 0.025 ml/ml, penicillin 100 U/mL, streptomycin 100 U/mL and 2.5 mM glucose). Explants were then bisected to create a pair of hemi-cylindrical samples.

Fluorescence Assay of Cellular Function

To observe mitochondrial function and cell death, paired hemi-cylinders were stained with a 3-color fluorescence assay: (1) tetramethylrhodamine, methyl ester (TMRM 10nM; 30 minute incubation), which concentrates in mitochondria based on the proton
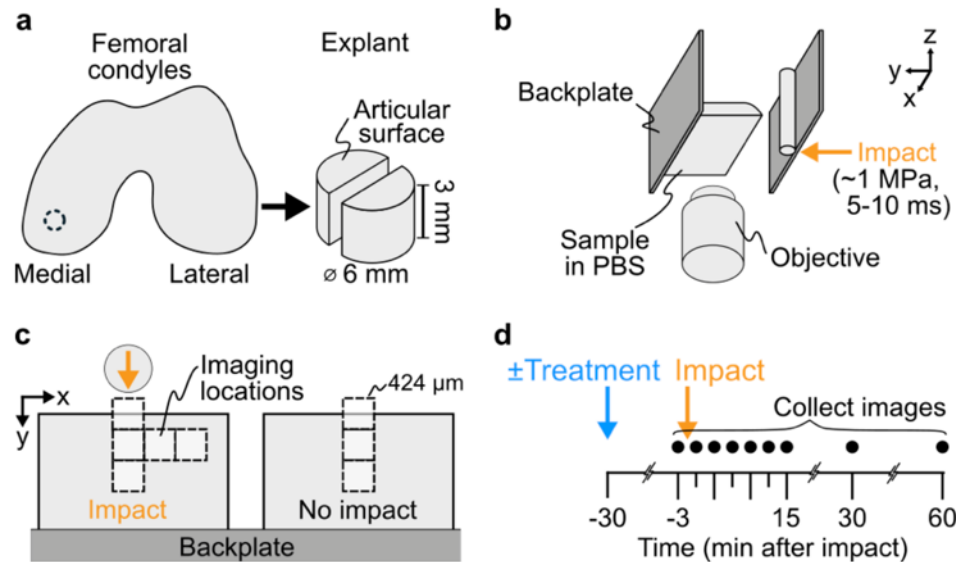
Figure 1. Experimental methods. (a) Cylindrical explants were dissected from medial condyles of bovine stifles and bisected to created paired samples. (b) Samples were stained with a 3-color assay for mitochondrial polarity and mounted to the stable backplate of a custom impactor. This test frame was subsequently mounted on a confocal microscope. (c) Paired hemi-cylindrical samples were mounted side-by-side on the backplate such that the two were in the same fluid bath but only one was impacted, while the second served as a non-impacted control. Samples were imaged at various locations relative to the impact (8 square fields of view; 5 on the impacted sample, 3 on the non-impacted sample). (d) Samples were imaged at all locations longitudinally, including before and up to 60 minutes after impact. For treated samples, SS-31 peptide treatment was added to the PBS bath surrounding both hemi-cylinders 30 minutes before the first image.

gradient across the inner membrane, reflecting mitochondrial polarity; (2) MitoTracker Green (200nM, for 50 minutes), which localizes to all mitochondria regardless of polarity; (3) Sytox Blue (100nM for 30 minutes), a cell-impermeant nucleic acid stain to identify dead cell nuclei (ThermoFisher Scientific, Waltham, MA). Paired hemi-cylinders were mounted side-by-side to the impactor backplate (Figure 1), as described previously[36] and suspended in PBS containing Sytox Blue, to ensure that cells dying during the experiment would take-up stain. A series of preliminary studies were conducted to validate this experimental system (*see Supplementary Materials)*. In a

subset of experiments, SS-31 (1 µM; provided by H. Szeto) was added and samples sat unperturbed in the bath for 30 minutes prior to injury.

Cartilage Injury

Cartilage was injured using a custom impacting device that utilizes a spring-loaded piston to deliver an energy-controlled impact.[36, 37] Paired hemi-cylindrical samples were mounted such that one served as a no-impact control, while the second was centered in the path of an 8mm diameter stainless-steel rod (Figure 1c). Based on previous characterization, this impact induced a peak stress of ~1 MPa and lasted about 5-10ms, producing a loading rate and magnitude of tissue-level strains comparable to what may be experienced *in vivo* during injurious, super-physiologic loading.[33] However, it is important to note that this impact geometry was not designed to reproduce any specific clinical loading scenario, but to expose tissues to a wide range of spatially dependent strains (from non-injurious to injurious) within in a relatively small field of view, enabling correlations between cellular function and injury mechanics to be rigorously investigated.

Confocal Imaging

To image the fluorescence assay longitudinally, the impact device, which includes a cover-glass window in the bottom, was mounted on an inverted, point-scanning confocal microscope (LSM 880, Zeiss, Oberkochen, Germany) with a 20× objective. This configuration allowed imaging of 424x424µm (1024 x1024 pixel) of the depth-profile of the samples (Figure 1b,c). Images were collected at 8 locations (5 fields on impacted hemi-cylinder, 3 on no-impact control), with the impact centered in the frame of the first image (Figure 1c). Combined, these images captured ~1 mm laterally from the impact

location on the articular surface to ~1 mm deep, and therefore included chondrocytes

from the superficial zone as well as deeper layers, but do not approach the region of the
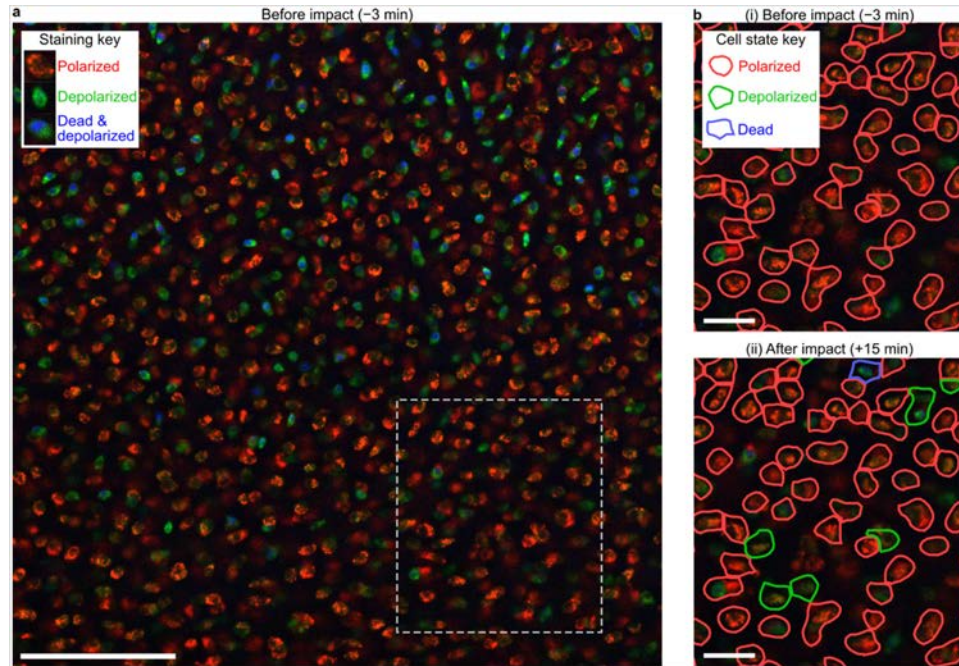

Figure 2. Image segmentation and cell classification. (a) An image taken at the first time point, immediately before impact, shows characteristic staining pattern. In this mitochondrial assay, red staining highlights polarized mitochondria, green staining highlights all mitochondria regardless of polarity, and blue staining highlights dead cell nuclei. Dashed rectangle indicates region highlighted in (b). Scale bar indicates 100 μm. (b) Images were subsequently analyzed to segment and classify cells as indicated by colored outlines. Cell state, as determined by the color distribution in each cell, is indicated by the color of the segmentation outline. (i) Only cells that had polarized mitochondria (red outlines) before impact were tracked longitudinally. (ii) Observing the same location at 15 minutes after impact, some cells changed from polarized to depolarized (green outline) or dead (blue outline). Scale bar indicates 25 μm.

neo-tidemark. Images were collected at 3 minutes pre-, and 0, 3, 6, 9, 12, 15, 30, and 60

minutes post-impact (Figure 1d). Time 0 imaging started <30 seconds after impact and

each image set took ~2 minutes to collect. Images were collected sequentially in three

channels corresponding to the three-stain assay (Figure 2a): TMRM (red; 561nm

excitation/563-735nm detection), MitoTracker (green; 488nm/499-553nm), Sytox (blue;

405nm/414-479nm).

Image Analysis

Confocal images were analyzed to extract individual-cell behavior over time using MATLAB (MathWorks, Waltham, MA). Analysis included three steps: registration, segmentation, and classification. At each time point, segmented cells were classified into one of 3 states: polarized mitochondria, depolarized mitochondria, or dead, based on stain intensity distribution within that cell (Figure 2). Density estimates were then used to compute local variations in fraction of cells in each state (see *Supplemental Methods*).

Electron Microscopy

To assess mitochondrial morphology and structure, two hemi-cylinder pairs were impacted as described, but without fluorescent staining. One pair was treated with SS-31 as above. Samples were incubated at room temperature for 30 minutes after impact, then fixed, processed and imaged using transmission electron microscopy (TEM; see *Supplemental Methods*).

Fast camera elastography

To investigate the role of mitochondria in mechanotransduction during injury, fast-camera elastography was used to track local strains in cartilage. Three hemi-cylindrical samples were coated with fluorescent microspheres, as described previously[37] and tested within 5 hours of dissection. Samples were impacted as described above, while being imaged with a high-speed camera (10× objective; v7.1, Vision Research, Wayne, NJ) and mercury arc lamp illumination (HBO 100, Carl Zeiss Inc., Germany), enabling epi-fluorescence microscopy at 4,000 frames/second. To calculate local strain tensors at peak indentation, videos were analyzed using 2D digital-image correlation tracking software (Ncorr; subset radius: 35px, subset spacing: 5px, strain radius: 5 points).[38] For each

independent strain tensor component, strain fields were shifted to place the point of impact at the origin. Barnes smoothing interpolation was implemented to compute the average strain field on the same 100 µm spatial grid used to compute cell state density estimates.[39] To relate cell state data with strain data, cells were binned in 2D, using the same spatial grid as for strain analysis. Average strain tensor and average fraction of cells in each state was calculated for each spatial bin.

Statistical analysis

Mixed-effects linear models (Table S3) were used to evaluate cell-state data and investigate trends across time, impact condition, treatment condition, and impact strain (see Supplemental Methods; Statistical Models). Models also included a random effect for source animal. Significance was set at $p<0.01$. For each model, the response variable was transformed to ensure normal residuals. When fitting, each model was reduced and residuals were checked for normality and homogeneity. After fitting, various statistical comparisons were evaluated using F-tests of the associated model contrasts with a Satterthwaite approximation for degrees of freedom. Because impact state and strain are not independent (no-impact samples have zero strain), three models were fit to evaluate different objectives while maintaining linear independence of the effect variables. Since all observed cells were functional before impact by definition, models were only fit to post-impact data, namely time 0-60 minutes. To evaluate temporal trends, two linear models were fit; one using *fraction of dysfunctional cells* as the response variable, the second using *fraction of dead cells*. To investigate the relationship between strain and depolarization, a linear mixed-effects model was fit to fractional depolarization from impacted samples only, including strain norm during impact but not impact state.

RESULTS

Temporal Evolution of Mitochondrial Depolarization and Cell Death After Impact

To study mitochondrial dysfunction after cartilage injury, we developed a functional assay to automatically track the fate of thousands of individual cells over time and space using computer vision, and applied this method in an established *ex vivo* injury model.[36, 37] Injured cartilage underwent a rapid and pronounced wave of mitochondrial depolarization, with the fraction of depolarized chondrocytes increasing sharply in the first 15 minutes post-impact, followed by a more gradual rise for the duration of the experiment (Figure 3). Cell death also increased gradually over the experiment, in agreement with previous results.[36] Indeed, both mitochondrial dysfunction and cell death were significantly increased after impact compared to no-impact controls ($p < 1.2 \times 10^{-6}$ for $t \geq 0$min; 34-46% higher for depolarization, 1-14% for cell death). As expected, no-impact controls showed only slight depolarization at the end of the experiment and negligible cell death throughout ($p > 0.01$ for $t \geq 0$min).

The Effects of SS-31 on Chondrocyte Fate after Injury

Treatment with SS-31 peptide dramatically reduced both mitochondrial depolarization and cell death after impact (Figure 3; $p < 1.1 \times 10^{-3}$ for $t \geq 0$min and $p < 4.5 \times 10^{-3}$ for $t \subset [9, 30]$, respectively). For SS-31 treated samples, the level of dysfunction after impact was reduced to a level comparable to that of unimpacted, untreated controls (63% to 91% lower than impacted, untreated samples). In treated samples, impact still induced more mitochondrial dysfunction and cell death as compared to no impact ($p < 1.8 \times 10^{-8}$ for $t \geq 0$ min and $p < 2.6 \times 10^{-11}$ for $t \geq 3$ min, respectively), but this increase was small in magnitude (2-13% and 0-3%, respectively), and not different than unimpacted, untreated controls.
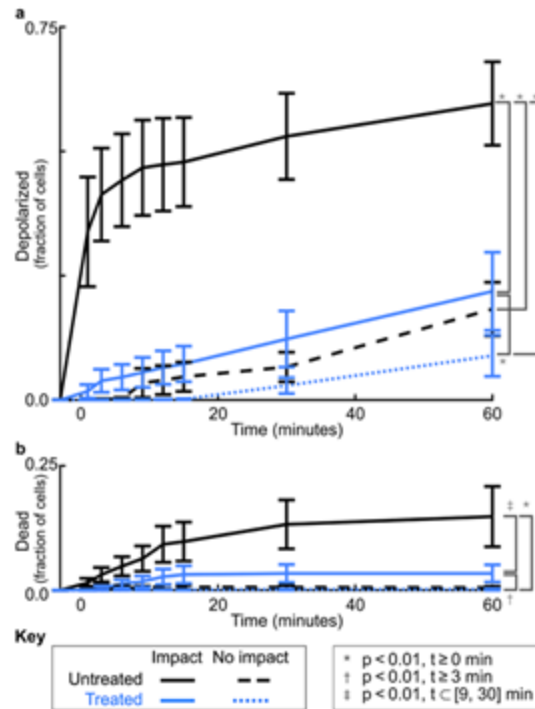
Figure 3. Mechanical impact induces rapid mitochondrial depolarization and gradual cell death that are both significantly reduced by SS-31 treatment. (a) Without treatment (black lines), the average fraction of cells with depolarized mitochondria increased dramatically in the first 15 minutes after impact and was higher in impacted samples as compared to non-impacted controls (p<1.3×10^{-4}). With treatment (blue lines), impacted samples showed dramatically less depolarization (p<1.1×10^{-4}), especially in the first 15 minutes, while non-impacted controls were unaffected by treatment (p>0.01). (b) Fractional cell death in impacted samples was smaller and increased gradually over time but was still significantly reduced by SS-31 treatment (p<4.5×10^{-4}, 9-30 min after impact). Points show the mean across samples (i.e. animals) and error bars indicate standard error of the mean. Untreated and treated results reflect the responses of samples from 5 and 4 animals, respectively. Statistical comparisons were evaluated using mixed-effects models (Supplementary Table S1, Supplementary Table S2).

Strain-dependence of peracute mitochondrial dysfunction

To investigate the role of mitochondria in mechanotransduction, we tested the hypothesis that mitochondria depolarization was correlated with local tissue strain during cartilage injury. At 15 minutes post-impact, the average fractional mitochondrial depolarization in untreated samples was highest near the impact location and decreased further away (Figure 4a). In contrast, samples treated with SS-31 peptide showed much less mitochondrial depolarization with no obvious spatial pattern (Figure 4b). The local average strain tensor field, as characterized by the Lagrange strain norm at peak indentation, was also highest near the impact and decreased further away (Figure 4b). Correlating mitochondrial dysfunction with impact strain revealed that without treatment, mitochondrial depolarization was highly correlated with Lagrange strain norm during impact (Figure 4c(i), black points; Pearson correlation coefficient R=0.68; mixed-model slope m=2.4; p=6.0×10^{-300} against null-hypothesis of zero strain dependence). In

contrast, SS-31 treatment not only reduced mitochondrial depolarization, but also eliminated the correlation between strain and depolarization, indicating that SS-31 targets mechanically-dependent mitochondrial dysfunction (Figure 4c(i), blue points; R=0.07; m=0.070; p=0.23 against null hypothesis of zero strain dependence; p=7.5×10^{-131} against null hypothesis of equal strain dependence regardless of treatment). All non-impacted samples experienced zero impact strain, by definition, and showed negligible mitochondrial depolarization with no obvious spatial pattern, as expected (Figure 4a,b,c(ii)). Full strain fields and time-dependent correlations are presented in Supplemental Figures S1 and S2. Collectively, these results demonstrate that mitochondrial function is strongly dependent on tissue strain and support the hypothesis that mitochondria mediate chondrocytes' immediate response to injury.
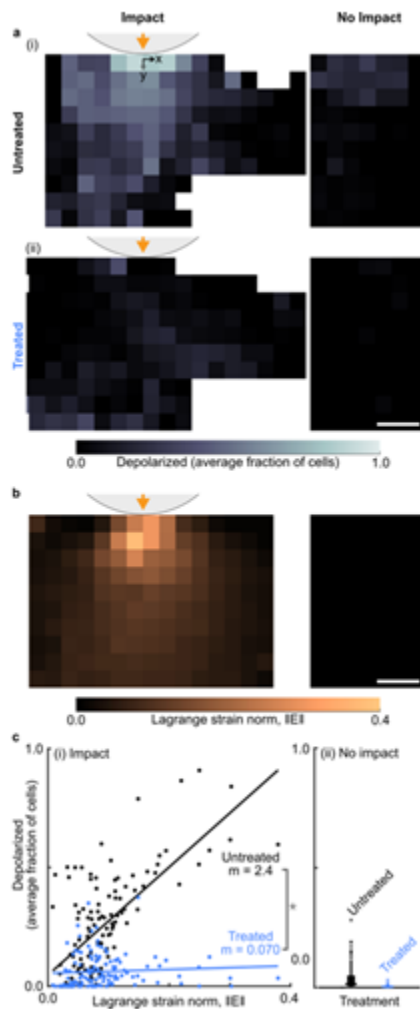

Figure 4. Treatment with SS-31 eliminates strain-induced mitochondrial depolarization. (a) (i) Without treatment, the local fraction of cells with depolarized mitochondria is high near the impact location and decreases farther away, while non-impacted samples show nearly zero depolarization. (ii) In contrast, samples treated with SS-31 show minimal depolarization after impact, while depolarization in non-impacted samples remains nearly zero. Scale bar indicates 250 μm. (b) At peak displacement during impact, Lagrange strain norm is highest near the impact and decreases further away, while no-impact samples have zero strain, by definition. Scale bar indicates 250 μm. (c) (i) In impacted but untreated samples, depolarization is correlated with the local strain (p=8×10^{-131}), but after SS-31 treatment this correlation is eliminated (p>0.01). Each point corresponds to one spatial bin. Lines indicate the best fit and m values indicate the associated strain-norm coefficients (i.e. slope). Note: * indicates significantly reduced strain correlation after treatment (p=2×10^{-131}). (ii) A Tukey box plot shows the distribution of fractional depolarization in non-impact samples (zero strain), which remains low for both treatment groups. All plots show depolarization at 15 minutes after impact and Lagrange strain at peak displacement during impact. Untreated and treated results reflect the response of paired samples from 5 and 4 animals, respectively. Statistical comparisons were evaluated using a mixed effects model (Supplementary Table S3).

Structural Changes in Mitochondria After Impact

Transmission electron microscopy (TEM) was used to investigate mitochondrial structure and morphology. Separate samples were impacted as described, without fluorescent

staining. As before, a subset of samples were treated with SS-31 prior to impact. Chondrocytes in no-impact samples displayed elongate mitochondrial morphology with distinct cristae structure in the inner mitochondrial membrane (Figure 5a). After impact, mitochondria were generally small and ovate, with little apparent cristae structure (Figure 5b). In contrast, samples treated with SS-31 maintained normal mitochondrial morphology and retained cristae structure after impact (Figure 5c).
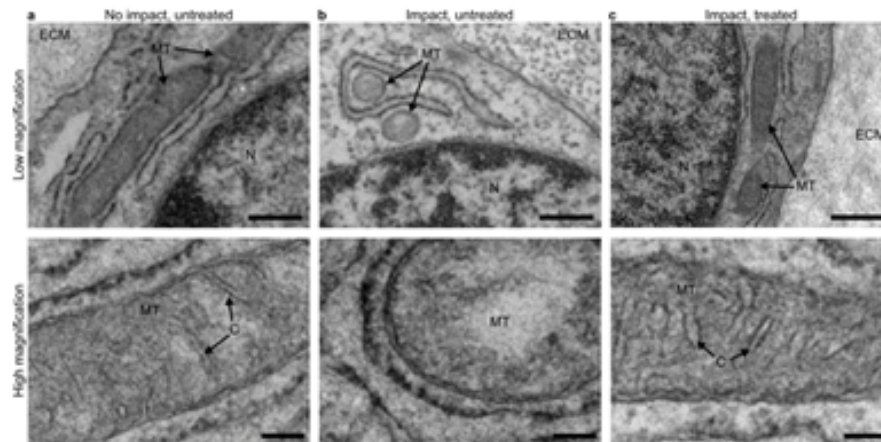

Figure 5. Electron microscopy reveals that SS-31 treatment preserves mitochondrial morphology. (a) Chondrocytes in an untreated, non-impact sample display normal, elongated mitochondrial morphology (top) and well-defined cristae structure (bottom). (b) After impact, untreated mitochondria appear ovate and lack cristae structure. (c) In contrast, samples treated with SS-31 have normal mitochondrial morphology with preserved cristae structure after impact. For imaging, samples were fixed 30 minutes after impact and images were collected in locations directly under the impact, corresponding to the imaging locations outlined in Figure 1c. Text and arrow labels on each image indicate extracellular matrix ("ECM"), mitochondria ("MT"), nucleus ("N"), and cristae ("C"). In low magnification images (top row) scale bar indicates 600 nm. In high magnification images (bottom row) scale bar indicates 200 nm.

DISCUSSION

Increasing evidence supports a role for mitochondria in early responses after cartilage injury, where mitochondrial dysfunction may act as a key driver of downstream catabolic

events, initiating and perpetuating tissue damage that leads to cartilage degeneration and ultimately PTOA.[15] Therefore, understanding how mechanical injury influences mitochondrial function has important implications for developing disease-modifying OA drugs. In this study, we tracked individual chondrocyte fate *in situ* after injury, and identified peracute strain-dependent mitochondrial dysfunction, and its prevention by the mitoprotective peptide, SS-31.

Results revealed that mitochondrial depolarization was increased over baseline at the first timepoint (t=0; ~0.5-2.5 minutes post-impact, see Methods), suggesting that mitochondrial dysfunction is one of the first consequences of injurious loading. This is faster than previous evidence of impact-induced mitochondrial dysfunction observed 2-6 hours after cartilage injury, where it was associated with increased proton leak and decreased ATP turnover, indicating increased mitochondrial membrane permeability and decreased ETC efficiency.[15] Our findings are in contrast to those of Huser and Davies, who impacted cartilage with similar energy but lower stress and observed depolarization at 3 and 6 hours, but not immediately after injury.[13] That study was in line with the known mechanism by which calcium overload causes mitochondrial depolarization.[25, 40] Our findings of immediate mitochondrial depolarization and high strain correlation imply that, at higher stress, peracute mitochondrial dysfunction can be attributed to local strain experienced during injury and thus may involve distinct mechanisms. Notably, while a large fraction of cells exhibited mitochondrial depolarization in the current study, a smaller fraction died, indicating a population of cells which could be rescued by therapeutic intervention.

In agreement with work in other models,[20, 22] our results demonstrate chondrocyte mitochondrial dysfunction is localized to regions of high tissue strain; In PRG4 knockout mice,[22] increased shear strains in the tissue were induced by increased friction due to the lack of lubricin.[22] In Bonnevie, et. al., different shear strains were superimposed on a similar compressive strain field,[20] while in the current work, impact loading created a complex loading pattern that includes both compressive and local strains. Although Waller, et. al. did not measure local tissue strains, Bonnevie et. al., and the current study measured the full 2D strain tensor in the tissue during loading, which enabled determination of the relationship between loading and mitochondrial response. In both cases, the combination of shear and compressive strains (represented by the norm of the strain tensor in the current study) was most predictive of mitochondrial dysfunction. Thus, while these studies induced different types of loading, all point to local tissue strain as a predictor of mitochondrial dysfunction.

To investigate if mitoprotection can prevent impact-induced mitochondrial dysfunction, we tested the effect of a cardiolipin-stabilizing peptide, SS-31. Our results showed that SS-31 treatment before impact dramatically reduced mitochondrial depolarization to levels comparable to unimpacted controls. Notably, treatment targeted mechanically-dependent depolarization, as evidenced by the loss of correlation with strain. Moreover, the beneficial effects of SS-31 were evident immediately after injury. While a recent study showed that SS-31 can reduce impact-induced chondrocyte apoptosis in the acute time frame (i.e. days),[15] the current study shows that pretreatment with peptide can dramatically reduce peracute (i.e. minutes to hours) mitochondrial depolarization and cell death. It is important to note that the goal of this study was not to prescribe a specific

dose or timing for mitoprotective therapy in vivo, but to investigate the effects of SS-31 on chondrocytes across a variety of mechanical conditions. Our previous work reported that the peptide diffuses rapidly through the depth of cartilage, localizes to chondrocyte mitochondria, and can prevent chondrocyte death and cartilage matrix degradation when administered up to 12 hours after injury (i.e. at 0, 1, 6 and 12 post-impact).[15] Furthermore, while the current model was designed to assess mitochondrial function in the peracute time frame following a single injurious episode, recent work suggests that articular injury inhibits cartilage lubricating mechanisms, and increased frictional coefficients due to inadequate lubrication are associated with strain-induced mitochondrial dysfunction and chondrocyte apoptosis.[20,22] Taken together these studies suggest that in vivo, mitochondrial dysfunction is not likely limited to the acute time frame after cartilage trauma, but rather continues throughout the course of ongoing cartilage degeneration.

Mitochondrial protection was supported by electron microscopy, which showed that preincubation with SS-31 preserved tubular morphology and cristae structure 30 minutes after impact. SS-31 has been reported to protect cristae architecture in many cell types,[41-43] but this is the first such evidence in chondrocytes. In other tissues, SS-31 is known to localize to the inner mitochondrial membrane, where it specifically binds to cardiolipin.[28] Cardiolipin's conical structure helps to maintain membrane curvature and organize respiratory complexes into supercomplexes to facilitate electron transfer in the ETC,[44] increase ATP production, and reduce electron leak.[27] Loss of christae structure is related to impaired cellular metabolism and increased reactive oxygen species production.[44] Although not directly assessed in the current study, the mechanism of action of SS-31

related to cardiolipin has been elucidated in previous work; SS-31 prevents cardiolipin peroxidation and promotes cytochrome c retention, helping to protect mitochondria cristae structure, promote efficient ATP production, and prevent apoptosis and other downstream responses to cytochrome c release.[25, 27, 29] SS peptides can also prevent the degradation of OPA-1, a protein critical for cristae assembly.[29] Our results in chondrocytes are consistent with these known mechanisms of action, however these events presumably occur over many hours, so our finding of protection against immediate mitochondrial depolarization suggests a possible additional mechanism: namely, a role in maintaining inner mitochondrial membrane polarity during rapid mechanical stress. More broadly, these data support the idea that preserving mitochondrial structure is a promising therapeutic target for preventing mechanically-induced cartilage injury.

Together with previous studies, our observations support the role of mitochondria in mechanotransduction during cartilage injury. Given the time frame established in this study, both diffusible factors and physical communication of strain to mitochondria could play a role. Cellular strain can alter intracellular Ca^{+2} signaling, which is important for cartilage's injury response.[45, 46] Recent work demonstrated the existence of high-strain-sensing piezo channels that are functionally linked to the cytoskeleton in chondrocytes, such that cell strain results in cellular Ca^{+2} influx and chondrocyte death.[47] During cell stress, mitochondria play a protective role, buffering rapid shifts in intracellular Ca^{+2} by absorbing the excess and transiently storing it to maintain homeostasis.[48] Over a critical threshold, intra-mitochondrial Ca^{+2} induces mitochondrial transition pores to open, causing depolarization, mitochondrial dysfunction and cell death.[13, 49] Such signaling is known to induce mitochondrial swelling within 10 minutes after traumatic brain injury

(TBI),[49] similar to the injury-induced morphological changes observed here. In TBI, these consequences can be reversed if mitochondrial dysfunction is addressed early.[49] Similarly, our findings suggest that mechanically-induced mitochondrial dysfunction in cartilage may represent an important opportunity for mitoprotective intervention.

In addition to the known mechanisms of calcium signaling, our observations of immediate depolarization and high strain correlation suggest that mitochondria may be directly involved in mechanosensing during cartilage injury. Compressing the cartilage extracellular matrix induces cellular-level strain, and distorts the mitochondrial matrix.[17, 18, 50] Cytoskeletal elements can also transfer strain directly to mitochondria.[51] Although little is known about mitochondria mechanobiology, recent work revealed mechanosensitive ion channels in the mitochondrial membrane that open in response lipid bilayer stretching, dissipating membrane potential in *Arabidopsis thaliana.*[52] Furthermore, calcium-sensitive potassium channels on the inner mitochondrial membrane of human glioma cells have been found to respond to mechanical stimulation and regulate mitochondrial membrane potential.[53] Our results are in line with such direct mitochondrial mechanosensing in chondrocytes and these open questions warrant further investigation.

Finally, our results demonstrate the utility of image tracking, segmentation, and classification techniques for advancing scientific knowledge with microscopy-based assays. These automated techniques enabled us to track thousands of individual cells over space and time, facilitating more powerful statistical analyses in concert with local mechanical measurements. Fluorescence microscopy assays are commonly employed to observe cells *in vitro* and *in situ*, and similar techniques using computer vision and

machine learning are broadly applicable for any study that uses microscopy and fluorescence to assay cellular function.

There are several limitations to consider with regard to this study. First, experiments were performed on neonatal bovine cartilage explants. As cartilage matures, properties of the extracellular matrix change, with increased collagen density, organization, and crosslinking.[54, 55] In the current study, the surface and middle zones of the cartilage were imaged. While the architecture of the immature bovine cartilage does not exactly match that of adult human, the most significant differences are noted in the deep zone, where neonatal tissue has no calcified cartilage (and hence no tidemark) and where the collagen is less well aligned. In contrast, the more superficial tissue is quite similar to adult human; We have previously shown that the mechanical properties of adult human and immature bovine cartilage are similar to a depth of ~1500μm from the articular surface.[56] The local collagen and proteoglycan concentrations in this region are also similar to those observed in adult human cartilage.[58] Furthermore, we have previously demonstrated that injury induces mitochondrial dysfunction, apoptosis, and cell death in both adult and immature cartilage, and these cellular responses can be rescued by treatment with SS-31.[15]

Another limitation is the environmental conditions during imaging. The current experiments were performed at 21% oxygen concentration [O_2], which is considered relative hyperoxia for normal cartilage.[59] Although there is disagreement in the literature regarding the effects of O_2 on mitochondrial function, between 5 and 21% O_2, mitochondrial function in cartilage explants was relatively constant, and independent of [O_2] and glucose in short-term (48 hour) chondrocyte culture.[60-63] Furthermore, although

5% is often considered physiologic for normal cartilage, it is unclear what O_2 environment chondrocytes experience in vivo after traumatic injury, where hemarthrosis is common and bleeding from subchondral bone or joint capsule can result in admixture of blood with 95-100% O_2 saturation.[64] The current study was conducted at 21% O_2 to be consistent with recent work linking cartilage impact to mitochondrial dysfunction[12] and the chondroprotective effects of SS-31 in injured cartilage explants.[15] Additional studies are warranted to investigate the effects of mitoprotection at various oxygen concentrations ex vivo.

Finally, it is important to note that the impact geometry in this study was not designed to reproduce any specific clinical loading scenario, it was intentionally designed to impose a wide range of strains (from 0 far from the impact to >0.4 under the impactor) in a relatively small field of view with high spatiotemporal resolution. Physiologic loading would induce a different distribution of strains in the tissue, but the response of cells to the microscale strain in their surroundings would not be expected to change. The strength of this experimental setup is that it allows us to directly observe local tissue strain and track the immediate live-cell responses of thousands of individual chondrocytes, while the cells are still embedded in their inhomogeneous peri- and extra-cellular matrices. Combined, this experimental design enables us to explore the underlying relationship between impact strain and cellular dysfunction, including mitochondrial depolarization and cell death.

By combining advanced techniques to understand local mechanics and cellular dysfunction, this study revealed the vital role of mitochondria in mediating cartilage's peracute response to traumatic injury. Our results show that mitochondria dysfunction

immediately after injury, are central to chondrocyte's response to trauma and that mitoprotection via SS-31 presents a promising therapeutic strategy. Collectively, this study of rapid impact mechanics and peracute mitochondrial dysfunction in cartilage is an important step toward understanding the pathogenesis of post-traumatic osteoarthritis and targeting mitochondria for treatment.

ACKNOWLEDGEMENTS

REFERENCES

1.   Cheng DS, Visco CJ. 2012. Pharmaceutical therapy for osteoarthritis. Pm r 4:S82-88.

2.   Gallagher B, Tjoumakaris FP, Harwood MI, et al. 2015. Chondroprotection and the prevention of osteoarthritis progression of the knee: a systematic review of treatment agents. Am J Sports Med 43:734-744.

3.   Mow VC, Ratcliffe A, Poole AR. 1992. Cartilage and diarthrodial joints as paradigms for hierarchical materials and structures. Biomaterials 13:67-97.

4.   Kühn K, D'Lima DD, Hashimoto S, et al. 2004. Cell death in cartilage. Osteoarthritis Cartilage 12:1-16.

5.   Del Carlo M, Jr., Loeser RF. 2008. Cell death in osteoarthritis. Curr Rheumatol Rep 10:37-42.

6.   Grodzinsky AJ, Levenston ME, Jin M, et al. 2000. Cartilage tissue remodeling in response to mechanical forces. Annu Rev Biomed Eng 2:691-713.

7.   Goldring MB, Goldring SR. 2010. Articular cartilage and subchondral bone in the pathogenesis of osteoarthritis. Ann N Y Acad Sci 1192:230-237.

8.   Anderson DD, Chubinskaya S, Guilak F, et al. 2011. Post-traumatic osteoarthritis: improved understanding and opportunities for early intervention. J Orthop Res 29:802-809.

9.   Blanco FJ, Rego I, Ruiz-Romero C. 2011. The role of mitochondria in osteoarthritis. Nat Rev Rheumatol 7:161-169.

10.   Terkeltaub R, Johnson K, Murphy A, et al. 2002. Invited review: the mitochondrion in osteoarthritis. Mitochondrion 1:301-319.

11. Goetz JE, Coleman MC, Fredericks DC, et al. 2017. Time-dependent loss of mitochondrial function precedes progressive histologic cartilage degeneration in a rabbit meniscal destabilization model. J Orthop Res 35:590-599.

12. Delco ML, Bonnevie ED, Bonassar LJ, et al. 2018. Mitochondrial dysfunction is an acute response of articular chondrocytes to mechanical injury. J Orthop Res 36:739-750.

13. Huser CA, Davies ME. 2007. Calcium signaling leads to mitochondrial depolarization in impact-induced chondrocyte death in equine articular cartilage explants. Arthritis Rheum 56:2322-2334.

14. Koike M, Nojiri H, Ozawa Y, et al. 2015. Mechanical overloading causes mitochondrial superoxide and SOD2 imbalance in chondrocytes resulting in cartilage degeneration. Sci Rep 5:11722.

15. Delco ML, Bonnevie ED, Szeto HS, et al. 2018. Mitoprotective therapy preserves chondrocyte viability and prevents cartilage degeneration in an ex vivo model of posttraumatic osteoarthritis. J Orthop Res.

16. Brouillette MJ, Ramakrishnan PS, Wagner VM, et al. 2014. Strain-dependent oxidant release in articular cartilage originates from mitochondria. Biomech Model Mechanobiol 13:565-572.

17. Knight MM, Bomzon Z, Kimmel E, et al. 2006. Chondrocyte deformation induces mitochondrial distortion and heterogeneous intracellular strain fields. Biomech Model Mechanobiol 5:180-191.

18. Szafranski JD, Grodzinsky AJ, Burger E, et al. 2004. Chondrocyte mechanotransduction: effects of compression on deformation of intracellular organelles and relevance to cellular biosynthesis. Osteoarthritis Cartilage 12:937-946.

19. Li D, Xie G, Wang W. 2012. Reactive oxygen species: the 2-edged sword of osteoarthritis. Am J Med Sci 344:486-490.

20. Bonnevie ED, Delco ML, Bartell LR, et al. 2018. Microscale frictional strains determine chondrocyte fate in loaded cartilage. J Biomech 74:72-78.

21. Kapitanov GI, Ayati BP, Martin JA. 2017. Modeling the effect of blunt impact on mitochondrial function in cartilage: implications for development of osteoarthritis. PeerJ 5:e3468.

22. Waller KA, Zhang LX, Jay GD. 2017. Friction-Induced Mitochondrial Dysregulation Contributes to Joint Deterioration in Prg4 Knockout Mice. Int J Mol Sci 18.

23. Coleman MC, Goetz JE, Brouillette MJ, et al. 2018. Targeting mitochondrial responses to intra-articular fracture to prevent posttraumatic osteoarthritis. Sci Transl Med 10.

24. Chan DC. 2006. Mitochondrial fusion and fission in mammals. Annu Rev Cell Dev Biol 22:79-99.

25. Szeto HH. 2014. First-in-class cardiolipin-protective compound as a therapeutic agent to restore mitochondrial bioenergetics. Br J Pharmacol 171:2029-2050.

26. Szeto HH, Birk AV. 2014. Serendipity and the discovery of novel compounds that restore mitochondrial plasticity. Clin Pharmacol Ther 96:672-683.

27. Birk AV, Chao WM, Bracken C, et al. 2014. Targeting mitochondrial cardiolipin and the cytochrome c/cardiolipin complex to promote electron transport and optimize mitochondrial ATP synthesis. Br J Pharmacol 171:2017-2028.

28. Birk AV, Liu S, Soong Y, et al. 2013. The mitochondrial-targeted compound SS-31 re-energizes ischemic mitochondria by interacting with cardiolipin. J Am Soc Nephrol 24:1250-1261.

29. Birk AV, Chao WM, Liu S, et al. 2015. Disruption of cytochrome c heme coordination is responsible for mitochondrial injury during ischemia. Biochim Biophys Acta 1847:1075-1084.

30.   Gibson CM, Giugliano RP, Kloner RA, et al. 2016. EMBRACE STEMI study: a Phase 2a trial to evaluate the safety, tolerability, and efficacy of intravenous MTP-131 on reperfusion injury in patients undergoing primary percutaneous coronary intervention. Eur Heart J 37:1296-1303.

31.   Saad A, Herrmann SMS, Eirin A, et al. 2017. Phase 2a Clinical Trial of Mitochondrial Protection (Elamipretide) During Stent Revascularization in Patients With Atherosclerotic Renal Artery Stenosis. Circ Cardiovasc Interv 10.

32.   Szeto HH. 2018. Stealth Peptides Target Cellular Powerhouses to Fight Rare and Common Age-Related Diseases. Protein Pept Lett 25:1108-1123.

33.   Aspden R. 2002. Letter to the Editor. Osteoarthritis and Cartilage. pp. 588-589.

34.   Schinagl RM, Gurskis D, Chen AC, et al. 1997. Depth-dependent confined compression modulus of full-thickness bovine articular cartilage. J Orthop Res 15:499-506.

35.   Buckley MR, Bonassar LJ, Cohen I. 2013. Localization of viscous behavior and shear energy dissipation in articular cartilage under dynamic shear loading. J Biomech Eng 135:31002.

36.   Bartell LR, Fortier LA, Bonassar LJ, et al. 2015. Measuring microscale strain fields in articular cartilage during rapid impact reveals thresholds for chondrocyte death and a protective role for the superficial layer. J Biomech 48:3440-3446.

37.   Henak CR, Bartell LR, Cohen I, et al. 2017. Multiscale Strain as a Predictor of Impact-Induced Fissuring in Articular Cartilage. J Biomech Eng 139.

38.   Blaber J, Adair B, Antoniou A. 2015. Ncorr: Open-Source 2D Digital Image Correlation Matlab Software. Experimental Mechanics 55:1105-1122.

39.   Scorer RS. 1992. Atmospheric data analysis, Roger Daley, Cambridge Atmospheric and Space Science Series, Cambridge University Press, Cambridge,

1991. No. of pages: xiv + 457. Price: £55–00, US$79–50 (hardback) ISBN 0521 382157. International Journal of Climatology 12:763-764.

40. Goldstein JC, Muñoz-Pinedo C, Ricci JE, et al. 2005. Cytochrome c is released in a single step during apoptosis. Cell Death Differ 12:453-462.

41. Szeto HH, Liu S, Soong Y, et al. 2015. Improving mitochondrial bioenergetics under ischemic conditions increases warm ischemia tolerance in the kidney. Am J Physiol Renal Physiol 308:F11-21.

42. Szeto HH, Liu S, Soong Y, et al. 2017. Mitochondria Protection after Acute Ischemia Prevents Prolonged Upregulation of IL-1beta and IL-18 and Arrests CKD. J Am Soc Nephrol 28:1437-1449.

43. Szeto HH, Liu S, Soong Y, et al. 2016. Protection of mitochondria prevents high-fat diet-induced glomerulopathy and proximal tubular injury. Kidney Int 90:997-1011.

44. Cogliati S, Enriquez JA, Scorrano L. 2016. Mitochondrial Cristae: Where Beauty Meets Functionality. Trends Biochem Sci 41:261-273.

45. Roberts SR, Knight MM, Lee DA, et al. 2001. Mechanical compression influences intracellular Ca2+ signaling in chondrocytes seeded in agarose constructs. J Appl Physiol (1985) 90:1385-1391.

46. Guilak F, Zell RA, Erickson GR, et al. 1999. Mechanically induced calcium waves in articular chondrocytes are inhibited by gadolinium and amiloride. J Orthop Res 17:421-429.

47. Lee W, Leddy HA, Chen Y, et al. 2014. Synergy between Piezo1 and Piezo2 channels confers high-strain mechanosensitivity to articular cartilage. Proc Natl Acad Sci U S A 111:E5114-5122.

48. Williams GS, Boyman L, Chikando AC, et al. 2013. Mitochondrial calcium uptake. Proc Natl Acad Sci U S A 110:10479-10486.

49. Sullivan PG, Thompson MB, Scheff SW. 1999. Cyclosporin A attenuates acute mitochondrial dysfunction following traumatic brain injury. Exp Neurol 160:226-234.

50. Sauter E, Buckwalter JA, McKinley TO, et al. 2012. Cytoskeletal dissolution blocks oxidant release and cell death in injured cartilage. J Orthop Res 30:593-598.

51. Ohashi T, Hagiwara M, Bader DL, et al. 2006. Intracellular mechanics and mechanotransduction associated with chondrocyte deformation during pipette aspiration. Biorheology 43:201-214.

52. Lee CP, Maksaev G, Jensen GS, et al. 2016. MSL1 is a mechanosensitive ion channel that dissipates mitochondrial membrane potential and maintains redox homeostasis in mitochondria during abiotic stress. Plant J 88:809-825.

53. Walewska A, Kulawiak B, Szewczyk A, et al. 2018. Mechanosensitivity of mitochondrial large-conductance calcium-activated potassium channels. Biochim Biophys Acta Bioenerg 1859:797-805.

54. Roth V, Mow VC. 1980. The intrinsic tensile behavior of the matrix of bovine articular cartilage and its variation with age. J Bone Joint Surg Am 62:1102-1117.

55. Lewis JL, Johnson SL. 2001. Collagen architecture and failure processes in bovine patellar cartilage. J Anat 199:483-492.

56. Buckley MR, Bergou AJ, Fouchard J, et al. 2010. High-resolution spatial mapping of shear properties in cartilage. J Biomech 43:796-800.

57. Silverberg JL, Barrett AR, Das M, et al. 2014. Structure-function relations and rigidity percolation in the shear properties of articular cartilage. Biophys J 107:1721-1730.

58. Bi X, Yang X, Bostrom MP, et al. 2006. Fourier transform infrared imaging spectroscopy investigations in the pathogenesis and repair of cartilage. Biochim Biophys Acta 1758:934-941.

59. Rajpurohit R, Koch CJ, Tao Z, et al. 1996. Adaptation of chondrocytes to low oxygen tension: relationship between hypoxia and cellular metabolism. J Cell Physiol 168:424-432.

60. Ströbel S, Loparic M, Wendt D, et al. 2010. Anabolic and catabolic responses of human articular chondrocytes to varying oxygen percentages. Arthritis Res Ther 12:R34.

61. Schneider N, Mouithys-Mickalad A, Lejeune JP, et al. 2007. Oxygen consumption of equine articular chondrocytes: Influence of applied oxygen tension and glucose concentration during culture. Cell Biol Int 31:878-886.

62. Zhou S, Cui Z, Urban JP. 2004. Factors influencing the oxygen concentration gradient from the synovial surface of articular cartilage to the cartilage-bone interface: a modeling study. Arthritis Rheum 50:3915-3924.

63. Grimshaw MJ, Mason RM. 2000. Bovine articular chondrocyte function in vitro depends upon oxygen tension. Osteoarthritis Cartilage 8:386-392.

64. Clements KM, Burton-Wurster N, Lust G 2004. The spread of cell death from impact damaged cartilage: Lack of evidence for the role of nitric oxide and caspases. Osteoarthritis Cartilage 12(7):577-85.